Optimisation and control of a hydraulic power take-off unit for a wave energy converter in irregular waves

C.J. Cargo, A.R. Plummer, A.J. Hillis*

Department of Mechanical Engineering, University of Bath, Bath BA27AY

Abstract

The optimization of a wave energy converter (WEC) hydraulic power take-off (PTO) for sea states of varying wave amplitude, direction, and frequency is a significant problem. Sub-optimal configuration can result in very inefficient energy conversion [1], so understanding the design trade-offs is key to the success of the technology. This work focuses on a generic point absorber type WEC. Previous work by the authors [2] has considered the optimisation of this device for regular waves to gain an understanding of the fundamental issues. This work extends the analysis to the more realistic case of irregular waves. Simulations are performed using an irregular wave input to predict how the PTO will operate in real sea conditions. Work is also presented on a motor speed control strategy to maintain the maximum flow of electrical power to the grid, assuming the use of a doubly fed induction generator (DFIG). Finally, the sizing of key components in the PTO is considered in an attempt to maximise PTO efficiency and generated power.

Key words: wave energy, hydraulic PTO, efficiency, power optimization, irregular waves

*Corresponding author

Email address: a.j.hillis@bath.ac.uk (A.J. Hillis)

1. Introduction

This paper presents an investigation into the optimisation of a point absorber wave energy converter (WEC) hydraulic power take-off (PTO) for irregular waves. The paper is structured as follows. Section 2 presents background literature and previous work by the authors. Section 3 presents the hydrodynamics theory used to study the WEC. Section 4 describes the operation and theory of the PTO mechanism. Section 5 dsicusses the generation of irregular wave profiles. Section 6 describes the performance of the WEC and PTO under irregular wave input conditions. Section 7 discusses the optimisation of the PTO mechanism for irregular condtions, and sections 8 and 9 discuss and evaluate a motor speed control strategy to extract the maximum possible energy from the waves. Finally, section 10 provides conclusions.

2. Background

Previous work has focused on developing control methods for point absorbers to maximize the energy absorbed. Falcao [3] used a simplified hydraulic PTO unit connected to a point absorber to develop an algorithm to optimize the converter. The algorithm was shown to be weakly dependent on wave period and independent of wave height when simulated in real sea conditions and to produce power levels similar to a fully linear PTO unit. This work was continued in Falcao [4] to include a strategy for phase control by latching to increase the absorbed power further. In Babarit et al. [5] three different latching control strategies are compared to show their effectiveness in different sea states with all three strategies giving a considerably increased efficiency in irregular waves. In Yavuz et al. [6] work focuses on assessing the performance of a tuneable point absorber by trying to fulfil the condition of resonance by varying the PTO characteristics. Results showed a maximum power capture of 50 per cent of the rated power in regular waves. This work was continued in Yavuz et al. [7] with irregular waves to show that power capture can be maximized by continuously tuning the natural frequency of the device to the incoming wave frequency. More recently, in Folley and Whittaker [8], a new control method called active bipolar damping or declutching is proposed

which tries to shift the buoy's velocity so it is in phase with the wave force. When compared theoretically to other methods, it shows a higher power capture than optimum linear damping without the requirement of reactive energy storage. This control method has been investigated in Babarit et al. [9] using a hydraulic PTO and compared to a control method which tries to mimic the continuous behaviour of a viscous damper. Results show greater power levels from the declutching control method with the added advantage of requiring a less complex system. Most of these investigations use linearized models and do not consider real hydraulic circuits and components in their investigations.

3. Hydrodynamics of the WEC

A point absorber type device is used for this study and is the same as that used in [2]. A diagram of the heaving buoy is shown in Fig. 1. The governing equation of motion for the buoy in heave is

$$m\ddot{x} = f_h(t) + \Phi(t) \tag{1}$$

where m is the mass of the buoy, $\ddot{x}$ is the buoy's acceleration, $f_h(t)$ is the total wave force and $\Phi(t)$ is the mechanical force created by the PTO and moorings. As linear wave theory is assumed, the wave force can be decomposed as follows

$$f_h(t) = f_e(t) + f_r(t) + f_{hs}(t) \tag{2}$$

$f_e(t)$ is the excitation force produced by an incident wave on an otherwise fixed body. For a regular wave the excitation force is a harmonic function of time and can be written

$$f_e(t) = Re(F_e e^{j\omega t}) \tag{3}$$

where F_e is the complex excitation force amplitude. The excitation force is a sum of the incident and diffracted wave components. Falnes [10] suggests that, if the body is small compared to the incoming wavelength, the diffracted term can be neglected and the excitation force is simply equal to the incident wave component, which is known as the 'Froude-Krylov' force. Furthermore since the system is

linear and there is only a single degree of freedom, the excitation force amplitude is proportional to the wave amplitude such that

$$|F_e| = \Gamma(\omega)\frac{H}{2} \tag{4}$$

where H is the wave height and $\Gamma(\omega)$ is a real and positive excitation force coefficient which is dependent on the body's shape and the wave frequency, obtained from

$$\Gamma(\omega) = \left(\frac{2g^3\rho B(\omega)}{\omega^3}\right)^{0.5} \tag{5}$$

where $B(\omega)$ is the radiation damping co-efficient. For the assumed hemispherical body shape, Falnes [10] uses previous work by Hulme [11] to show that

$$B(\omega) \approx R_H e^{-2kl} \tag{6}$$

where R_H is the radiation damping coefficient for a semi-submerged sphere of radius a, given by

$$R_H = \omega\rho(\frac{2\pi}{3})a^3\epsilon \tag{7}$$

and ϵ is Havelock's dimensionless damping coefficient computed by Hulme [11]; $\epsilon = \epsilon(ka)$ and k is the wave number ($k = \frac{\omega^2}{g}$) given by the deep water dispersion equation.

$f_r(t)$ is the radiation force which is produced by an oscillating body creating waves on an otherwise calm sea. The radiation force can be decomposed into components in phase with the buoy's acceleration and velocity [10] [12] so that

$$f_r(t) = -A(\omega)\ddot{x} - B(\omega)\dot{x} \tag{8}$$

where $A(\omega)$ is the added mass coefficient. $f_{hs}(t)$ is the hydrostatic buoyancy force. For small heave displacements, which are expected, the hydrostatic force can be linearised so that

$$f_{hs}(t) = -\rho g S x \tag{9}$$

where ρ is the water density, g is the acceleration due to gravity and S is the buoy cross sectional area in the x-direction.

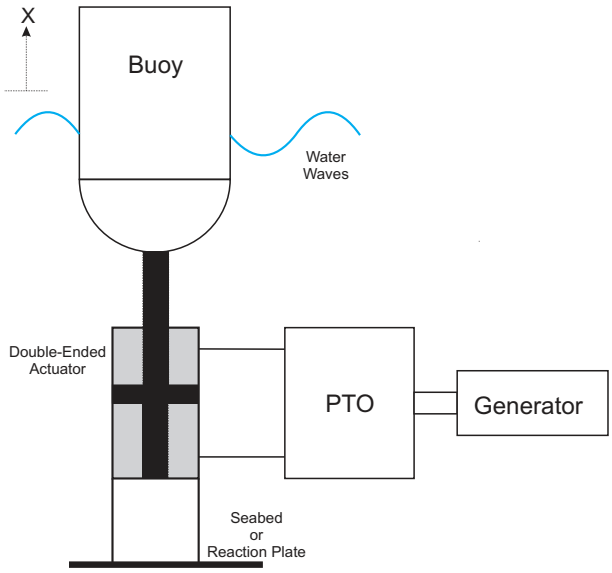

Figure 1: Schematic diagram of the WEC

4. Hydraulic PTO mechanism

Hydraulic PTOs are generally used in WECs due to their ability to deal with low frequency, high force wave inputs and their high power density and robustness. There is no standard configuration for a hydraulic PTO, with the design normally consisting of "sets of hydraulic cylinders that pump fluid, via control manifolds, into high pressure accumulators for short term energy storage. Hydraulic motors use the smooth supply of high-pressure fluid from the accumulators to drive grid-connected electric generators" [13]. The main aim of the PTO is to convert the irregular wave input into a smooth electrical power output by decoupling the power capture and power generation processes. This is achieved using accumulators for energy storage and means that the primary element of power capture can be sized to deal with the maximum power input, and the secondary element of power generation can be sized according to the average power capture and can therefore be smaller, cheaper and more efficient.

The hydraulic PTO used in this simulation model is shown in Figure 2. The simple circuit excludes components such as filters and coolers which would be required in the real hydraulic system. A rigid link between the buoy and the

PTO means that the motion of the buoy directly drives the double-acting equal area hydraulic piston working within a fixed cylinder. This motion drives fluid through a set of four check valves to rectify the flow so that fluid always passes through the hydraulic motor in the same direction (independent of the direction of the buoy motion). A high pressure accumulator is placed on the inlet to the hydraulic motor, and a low pressure accumulator on the outlet of the hydraulic motor. The pressure difference between the two accumulators drives a variable displacement motor, which is connected to an electrical generator. The accumulators are included to maintain an approximately constant pressure differential across the motor, assuming constant resistance, so it spins at a roughly constant speed and therefore power is generated at almost a constant rate. The thermodynamic transformations in the accumulators are assumed to be isentropic, which is reasonable considering the cycle time of the device. In this work, the generator is modelled as a simple rotational damper with varyiable damping coefficient allowing its resistive torque to be altered. In a real circuit, there will be external leakage from the motor to tank. Therefore, to replenish the circuit and avoid cavitation in the cylinder, a boost pump is required. This is incorporated with a pressure relief valve to maintain a minimum pressure in the system, which can be adjusted by varying the pressure relief valve setting. In this case the pressure relief valve is set to 10 bar.

In reality there will be losses throughout the hydraulic circuit such as friction in the piston, pressure losses in the pipes, leakage in the motor and torque losses due to friction in the motor and generator. These losses will depend on the specific operating conditions in the unit, which are determined by the size of certain components and the constantly changing wave conditions.

The PTO force is given by

$$\Phi = (p_1 - p_2)A_p - f_{fr} \tag{10}$$

where p_1 and p_2 are the pressures in the piston chambers, A_p is the piston area and f_{fr} is the cylinder friction force, given by

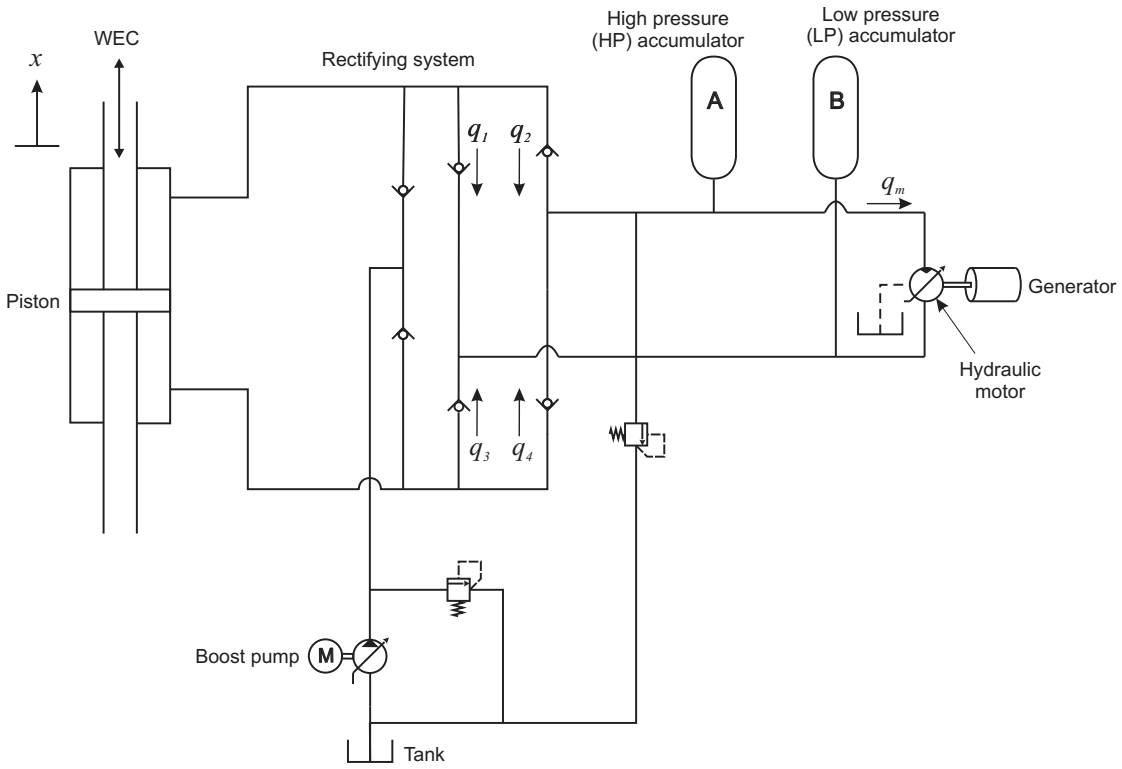

Figure 2: Hydraulic PTO circuit diagram

$$f_{fr} = f_c sign(\dot{x}) + f_v \dot{x} \tag{11}$$

where f_c and and f_v are the Coulomb and viscous friction coefficients, respectively.

The mechanical power captured by the PTO is given by

$$P_{cap} = \Phi \dot{x} \tag{12}$$

The pressures in the cylinder are determined by integrating the following cylinder flow equations:

$$A_p \dot{x} - q_1 - q_2 = \frac{V_1}{B_o} \frac{dp_1}{dt} \tag{13}$$

$$A_p \dot{x} - q_3 - q_4 = \frac{V_2}{B_o} \frac{dp_2}{dt} \tag{14}$$

where V_i is the volume of oil in piston chamber 'i = 1,2' including connected hydraulic lines, and B_o is the bulk modulus of the oil.

Check valve flows:

$$q_1 = \left\{ \begin{array}{rcl} 0 & : & p_1 > p_B \\ -K_v\sqrt{p_B - p_1} & : & p_B \geq p_1 \end{array} \right\} \tag{15}$$

$$q_2 = \left\{ \begin{array}{rcl} 0 & : & p_A > p_1 \\ K_v\sqrt{p_1 - p_A} & : & p_1 \geq p_A \end{array} \right\} \tag{16}$$

$$q_3 = \left\{ \begin{array}{rcl} 0 & : & p_2 > p_B \\ -K_v\sqrt{p_B - p_2} & : & p_B \geq p_2 \end{array} \right\} \tag{17}$$

$$q_4 = \left\{ \begin{array}{rcl} 0 & : & p_A > p_2 \\ K_v\sqrt{p_2 - p_A} & : & p_2 \geq p_A \end{array} \right\} \tag{18}$$

K_v is the valve coefficient. Flow to accumulator 'A':

$$q_A = q_2 + q_4 - q_m \tag{19}$$

Volume of oil in accumulator 'A':

$$V_A(t) = \int_0^t q_A dt \tag{20}$$

Flow to accumulator 'B':

$$q_B = q_m - q_1 - q_3 \tag{21}$$

Volume of oil in accumulator 'B':

$$V_B(t) = \int_0^t q_B dt \tag{22}$$

With isentropic compression, the pressure in each accumulator is given by:

$$p_A \left(V_0 - V_A\right)^\gamma = p_o V_o^\gamma \tag{23}$$

$$p_B \left(V_0 - V_B\right)^\gamma = p_o V_o^\gamma \tag{24}$$

where p_o is the pre-charge pressure and V_o is the volume of each accumulator and

γ is the adiabatic index. The motor losses have been approximated using the Wilson model [14] with three dimensionless coefficients: the slip coefficient (C_s), the viscous friction coefficient (C_v) and the coulomb friction coefficient (C_f). Flow to the hydraulic motor is given by

$$q_m - \frac{C_s x_m D_m (p_A - p_B)}{\mu} = D_m \omega_m \tag{25}$$

where D_m is the motor displacement, x_m is the fraction of displacement used, μ is the dynamic viscosity of the oil and ω_m is the motor speed.
The motor torque is given by

$$T_m = (1 - C_f) x_m D_m (p_A - p_B) - C_v D_m \mu \omega_m \tag{26}$$

resulting in rotational acceleration

$$\dot{\omega}_m = \frac{T_m - T_g}{J} \tag{27}$$

where J is the inertia of the generator.
Using a simple resistive model, the generator torque is given by

$$T_g = C_g \omega_m \tag{28}$$

where C_g is the damping coefficient of the generator. Mechanical power generated by the PTO can then be found from

$$P_{gen} = T_m \omega_m \tag{29}$$

and the hydraulic motor efficiency is given by

$$\eta_m = \frac{T_m \omega_m}{q_m (p_A - p_B)} \tag{30}$$

Table 1 shows the component parameters in the PTO. These values are not based on any specific design but are a representation of suitable sizing for the buoy size. In this idealised case the effect of the boost pump is neglected. Also only

electrical generator input power is presented i.e. the generator efficiency is not considered. The high pressure accumulator ('A') has a relatively low pre-charge pressure to ensure that it charges even in calm wave conditions. Table 2 shows the parameters of all the other components required to calculate the losses.

Maximum system pressure	350 bar
Equal area piston	
Area	$0.007\,\mathrm{m}^2$
Stroke Limit	$\pm 2.5\,\mathrm{m}$
HP Gas accumulator 'A'	
Pre-charge Pressure	30 bar
Volume	200 L
γ	1.4
LP Gas accumulator 'B'	
Pre-charge Pressure	10 bar
Volume	200 L
γ	1.4
Variable Displacement Motor	
Capacity	180 cc/rev
Displacement fraction (x_m)	1
Generator	
Damping coefficient	$2.5\,\mathrm{Nm/(rad/s)}$
Inertia	$2\,\mathrm{kgm}^2$
Oil Properties	
Viscosity	50 cSt
Density	$850\,\mathrm{kg/m}^3$

Table 1: PTO component values

Cylinder	
Coulomb friction (f_c)	3500 N
Viscous friction coefficient (f_v)	$100\,\mathrm{N/(m/s)}$
Variable Displacement Motor	
C_f	0.014
Check Valve	
Valve constant (K_v)	$8.5\times\ 10^{-6}$
Cracking Pressure	0.3 bar
Pipework	
Diameter (d)	50 mm
Total Length (l)	10 m

Table 2: PTO unit component loss parameters

5. Wave Spectra and Irregular Wave Profiles

Sea waves are random in nature but they can be analysed by assuming they consist of an infinite number of waves with different frequencies and directions. Wave spectra are created by decomposing an irregular wave profile into a number of component sinusoidal waves. The characteristics of the frequency spectra of sea waves is now well established and formulae have been developed by researchers such as Bretschneider, Pierson-Moskowitz, Hasselmann and Mitsuyasu [15]. Here the Pierson-Moskowitz spectrum is used [16], which is defined as:

$$S_n(\omega) = 5\pi^4 \frac{H_s^2}{T_p^4} \frac{1}{\omega^5} exp\left[-\frac{20\pi^4}{T_p^4}\frac{1}{\omega^4}\right] \tag{31}$$

Where ω is frequency, H_s is the significant wave height and T_p is the peak period. From the spectrum a finite number of sinusoidal waves can be created. Each individual wave component is created with its own amplitude and frequency characterised by the spectrum. Each sinusoidal wave is assigned with a random phase and the wave elevation time series is generated as a sum of the individual components according to:

$$\eta(t) = \sum_{i=1}^{n} \sqrt{2S_n(\omega_i)\Delta\omega}\sin(\omega_i t + \varphi_i) \tag{32}$$

where ω_i and φ_i are the frequency and random phase component of the ith wave, and $\Delta\omega$ is the frequency band calculated from:

$$\Delta\omega = \frac{\omega_{max}}{n} \tag{33}$$

where ω_{max} is the maximum frequency of the spectrum and n is the number of wave components. ω_{max}= 8π rad/s and n= 1280 will be used in the following work.

Using linear wave theory means that the excitation force is generated as a sum of the individual excitation wave force components. The excitation force of each component is calculated from

$$f_e(t) = \sum_{i=1}^{n} \Gamma(\omega_i)\sqrt{2S_n(\omega_i)\Delta\omega}\sin(\omega_i t + \varphi_i) \tag{34}$$

Figure 3 presents an example of a Pierson-Moskowitz spectrum and the corresponding wave elevation and force profile that is generated for $H_s = 3\,\mathrm{m}$ and $T_p = 10\,\mathrm{s}$.

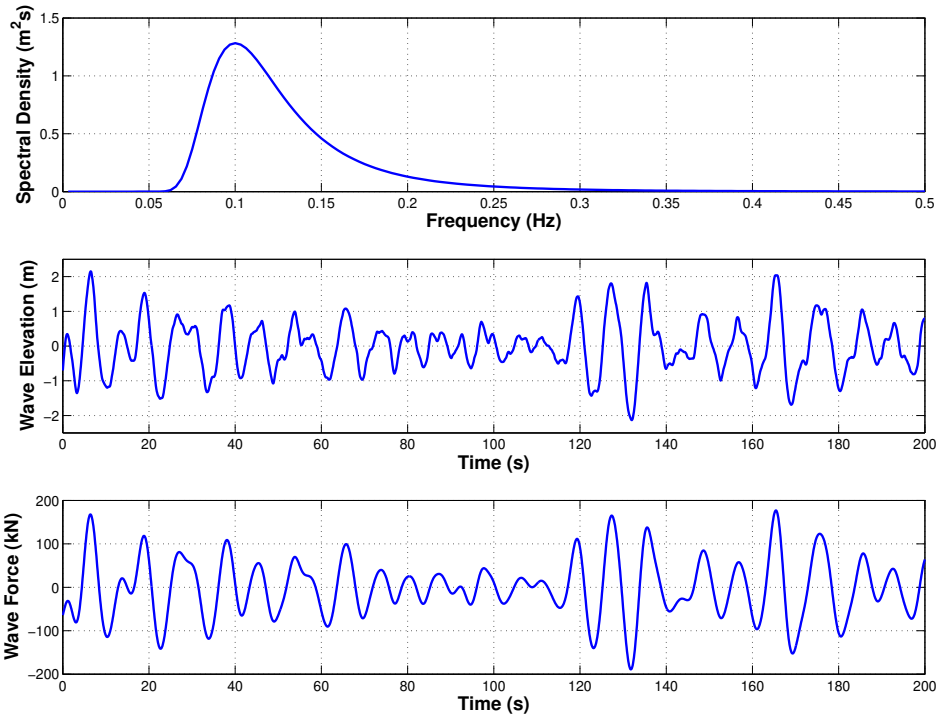

Figure 3: Top: Pierson Moskowitz Spectrum for $H_s = 3\,\mathrm{m}$ and $T_p = 10\,\mathrm{s}$, Middle: Wave surface elevation, Bottom: Wave Force

This is the random-phase method that has been used in previous work to represent irregular waves with good approximation [4]. There is another method which uses filtered white noise to represent a random sea profile. The filter is designed according to a specific spectrum as described in [17, 18].

6. WEC Behaviour

Using the wave profile from Figure 3, the simulation model was run for 200 s with full motor displacement to produce Figures 4 and 5.

The first noticeable characteristic is that the induced body stall is more pronounced than observed in regular waves [2] (e.g. 140 - 147 s). The WEC

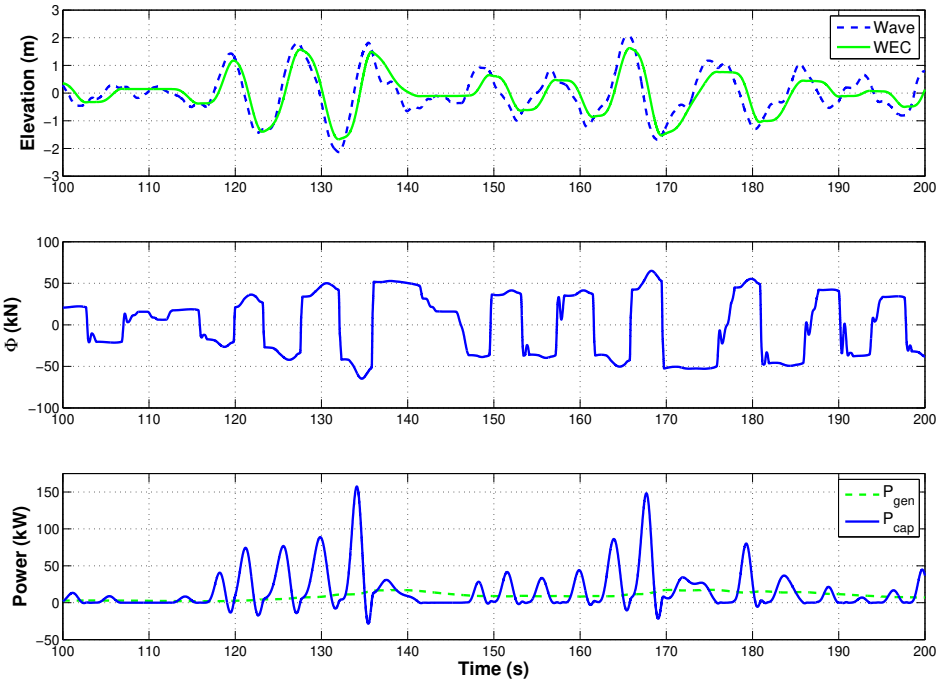

Figure 4: Top: Wave and WEC displacement. Middle: PTO force. Bottom: Power captured and generated. (H_s=3 m and T_p=10 s)

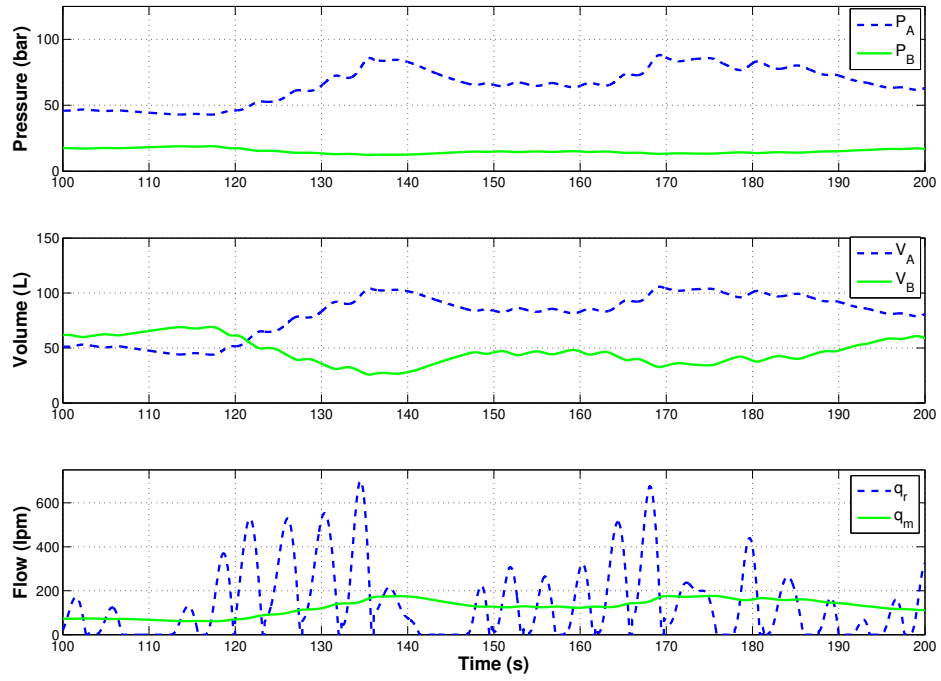

Figure 5: Top: High and Low Pressure line. Middle: Accumulator Volume. Bottom: Flow from rectifier and flow to motor. (H_s=3 m and T_p=10 s)

remains stationary during periods of small incident waves because insufficient force is produced to overcome the pressure in the high pressure accumulator. Furthermore, a number of consecutive large incident waves causes large WEC displacements, which increases system pressure and PTO force (e.g. 115 - 135 s). This emphasises the stall as upcoming waves, which may have been large enough to overcome the PTO force before are not large enough now. The PTO force still exhibits a square wave form (Figure 4) but its magnitude is variable due to the constantly varying system pressure. Also, the frequency of the square wave is variable as the duration of the body stall is continually changing.

The power smoothing effect of the accumulators is exhibited with the comparisons between P_{cap} and P_{gen} and the rectified flow (q_r) and the flow to the motor (q_m). P_{cap} has a maximum value of approximately 150 kW compared to 18 kW for P_{gen} which reinforces the importance of power smoothing in detaching the power capture element of the PTO from the power generating element. It means that the hydraulic motor and generator can be sized accordingly to be more efficient.

Although the accumulators are very large (200 L), the pseudo-steady state which is reached with regular waves does not exist in irregular waves. Therefore, it is necessary to examine the energy storage in the accumulators. The varying pressure and oil volumes in both accumulators are dependent on the incoming wave conditions. p_A and V_A increase from the initial values of 41 bar and 40 L respectively. There is also an increase in V_B but p_B remains approximately constant at 14 bar, just above the pressure relief valve setting of the boost pump. This means that some of the power captured by the PTO is stored in the accumulators as hydraulic energy instead of being turned into mechanical power that is generated by the motor. It is necessary to determine the additional hydraulic energy which is stored in the accumulators ($E_{A,B}$) and include this in the total power generated. Equations 35 - 39 show how the energy (E_m) and power (P_m) generated by the motor and the energy stored in the accumulators ($E_{A,B}$) are calculated and used to give total power P_{gen}. Table 3 displays the corresponding values for this simulation. It is understood that the additional accumulator energy is still subject to the inefficiencies of the motor when it is

recovered, but this loss is neglected in the Table.

$$E_A(t) = p_A(t)V_A(t) - p_A(0)V_A(0) \tag{35}$$

$$E_B(t) = p_B(t)V_B(t) - p_B(0)V_B(0) \tag{36}$$

$$E_m(t) = \int_0^t T_m\omega_m dt \tag{37}$$

$$P_m(t) = \frac{1}{t}\int_0^t T_m\omega_m dt \tag{38}$$

$$P_{gen} = \frac{E_A + E_B + E_m}{t} \tag{39}$$

Component	Energy (kJ)
E_m	1679
E_A	345
E_B	43
	Power (kW)
P_{cap}	14.1
P_m	8.4
P_{gen}	10.3
η_{pto}	73.1%

Table 3: Energy distribution in the PTO and Average Power Values for a 200 s simulation. (H_s=3 m and T_p=10 s)

Table 3 reveals that E_B is negligible and E_A is approximately 20% of E_m, which means that the PTO efficiency value (η_{pto}) is slightly higher than in reality. The wave profile which is generated from using the random-phase method is periodic over a time frame (Δt) which is dependent on the resolution (minimum frequency (ω_{min})) of the spectrum. Therefore, to negate the energy storage in the accumulators affecting η_{pto}, in the following sections the simulation model is run for a total of 640 s, which equates to two full wave cycles. The second full cycle of data is extracted and examined so that $E_{A,B} \approx 0$ and $P_{gen} \approx P_m$, which will produce a more realistic value of η_{pto}.

$$\Delta t = \frac{1}{\omega_{min}} = \frac{2\pi}{8\pi/1280} = 320\,s \tag{40}$$

Although not the case in these simulations, note that in more energetic seas, the system pressure may reach the maximum system pressure of 350 bar. This is more likely when a group of large waves occur in succession. This introduces another inefficiency in the PTO as hydraulic energy is wasted as it passes through the pressure relief valve to tank. However, this is required for safety purposes and to reduce the risk of component failure. It is expected that this loss will be minimal due to the rare wave conditions which cause these pressures.

7. PTO Tuning

In previous work by the authors [2], an effective damping term α was formulated as:

$$\alpha = \left(\frac{A_p}{D_m}\right)^2 C_g \tag{41}$$

where A_p ia the piston area, D_m is the motor displacement and C_g is the generator damping coefficient. This effective damping was optimised for energy absorption by adjusting the motor displacement. To maximise the power generated in irregular waves a similar condition of optimum PTO damping (α_{opt}) might exist as with regular waves . It is expected that α_{opt} would stall the device for an optimum average duration and this value would be dependent on T_p of the incoming waves. It might be expected that maximum power levels would be reduced in irregular waves compared to regular waves of the same energy [19] as the device will only be optimally tuned to the wave frequency corresponding to the highest energy.

In regular waves α_{opt} shows no variation with wave height [2] H_s. Figure 6 indicates that this relationship still holds true for irregular waves, though there are some noticeable differences. With irregular waves there is a negligible reduction in normalised power with H_s, compared to the more marked reduction in regular waves, but the normalised power is approximately 40% of the normalised power in regular waves. As with regular waves, α_{opt} is the same

whether optimising for P_{gen} or P_{cap} but the value (175 kNs/m) is lower compared to regular waves (225 kNs/m) with the same height and period. However, as with regular waves, η_{pto} remains approximately constant for all values of α.

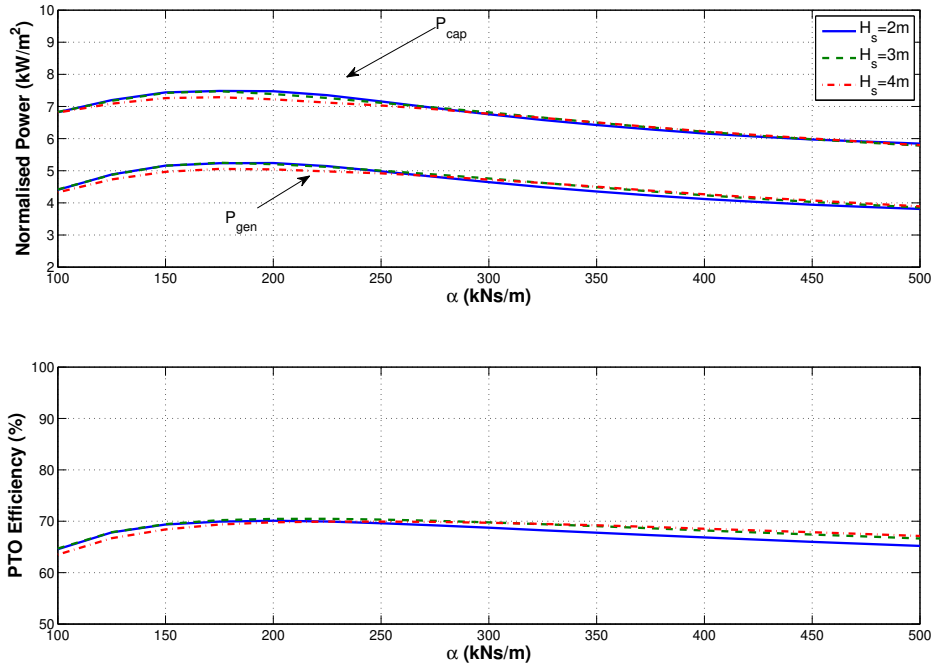

Figure 6: Normalised power and PTO efficiency vs PTO damping for varying significant wave heights and T_p=10 s

This result shows that, as with regular waves, the PTO can be tuned according to the wave profile by varying α in order to maximise power generation. Figure 7 indicates a linear relationship between T_p and the trend for α_{opt} in irregular waves but there is a larger deviation around this trend line compared to the regular wave results [2], due to the random nature of the waves.

In terms of power generation, Figure 8 reveals that P_{gen} does not reduce as markedly with T_p as in regular waves. P_{gen} is lower due to the inefficiencies of the PTO but the trend for P_{gen} and P_{cap} is almost identical which indicates a near constant PTO efficiency ($\eta_{pto} \approx 70\%$) for this range of T_p values at this H_s.

Figure 9 shows the response of an optimally tuned hydraulic PTO in the time domain for the same wave height and $T_p = 10$s.

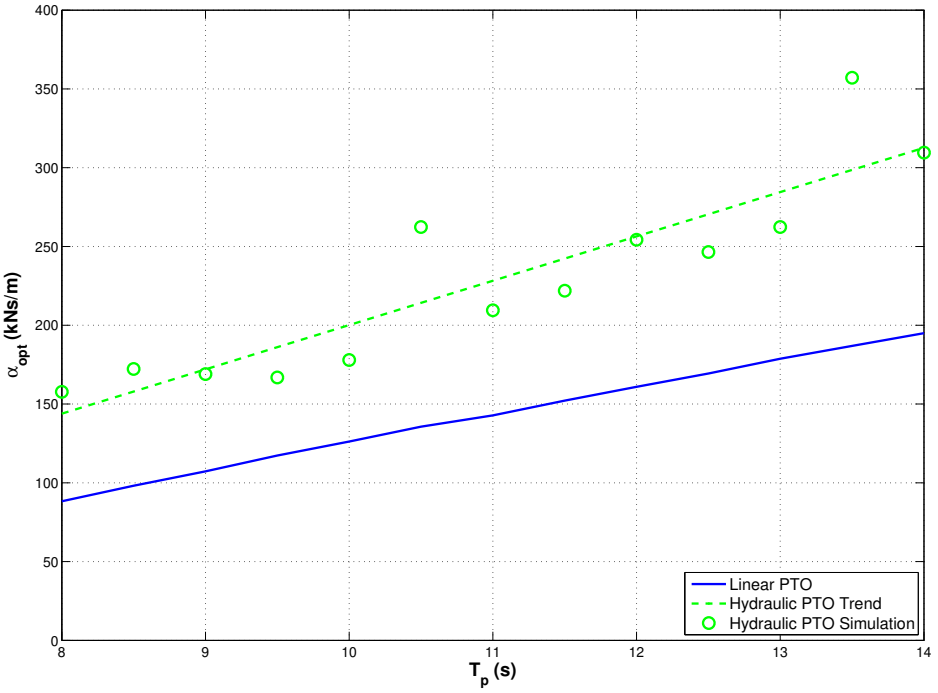

Figure 7: Optimum PTO damping vs peak wave period

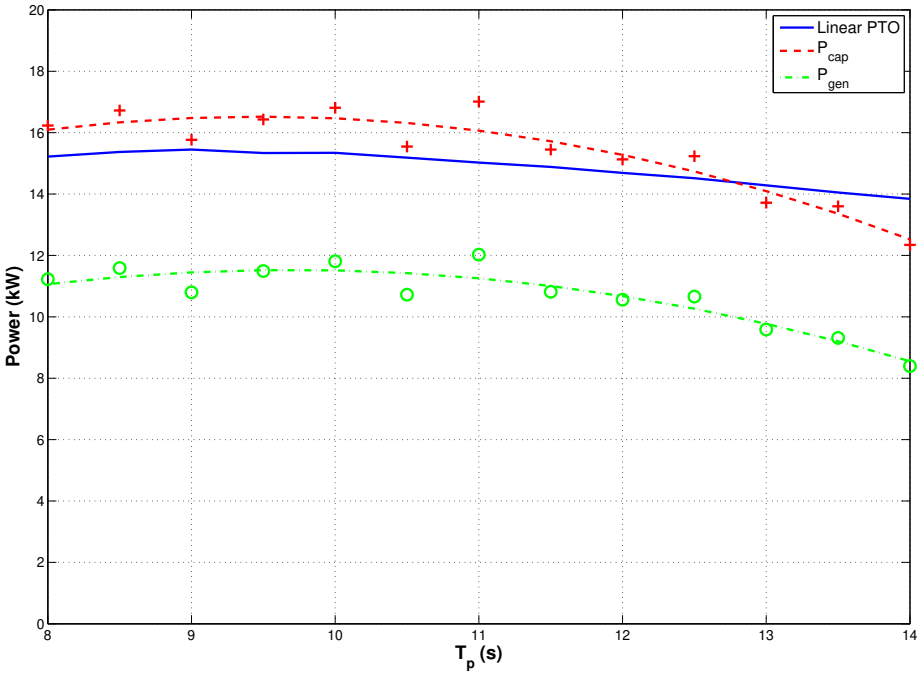

Figure 8: Maximum power generated vs peak wave period for H_s= 3m

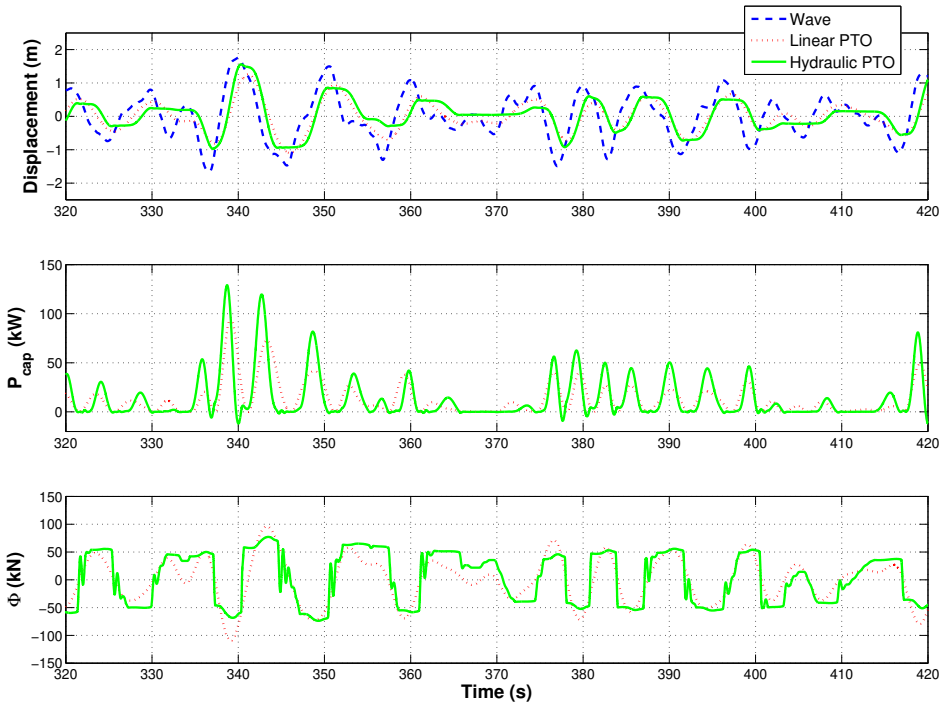

Figure 9: Comparison of the behaviour of an optimally tuned linear and hydraulic PTO in irregular waves. Top: WEC and Wave Displacement, Middle: Power Capture, Bottom: PTO Force. (H_s=3 m and T_p=10 s)

8. Motor Speed Control

Until now, it has been assumed that all the mechanical power produced by the hydraulic motor is converted into electrical power. No consideration has been given to how the PTO will be connected to the electrical grid and what type of generator will be used in the PTO. Wind turbines face the same challenge of variable speed operation and they often use DFIGs because they offer variable speed generation in an efficient manner by using a power electronic converter [20]. They have an operational range of about ±30% around the synchronous speed of 1500 rpm so it is assumed that if the hydraulic motor speed is outside of this range no power can be transmitted (P_{trans}) to the grid and the generated power is wasted. Within this range, P_{trans} is the generator input power, i.e. generator efficiency is not considered. Two further terms are introduced to analyse this effect; the transmission efficiency (η_{trans}) which is given by equation 42 and the total PTO efficiency (η_{tot}) which is given by equation 43.

$$\eta_{trans} = \frac{P_{trans}}{P_{gen}} \tag{42}$$

$$\eta_{tot} = \eta_{pto}\eta_{trans} \tag{43}$$

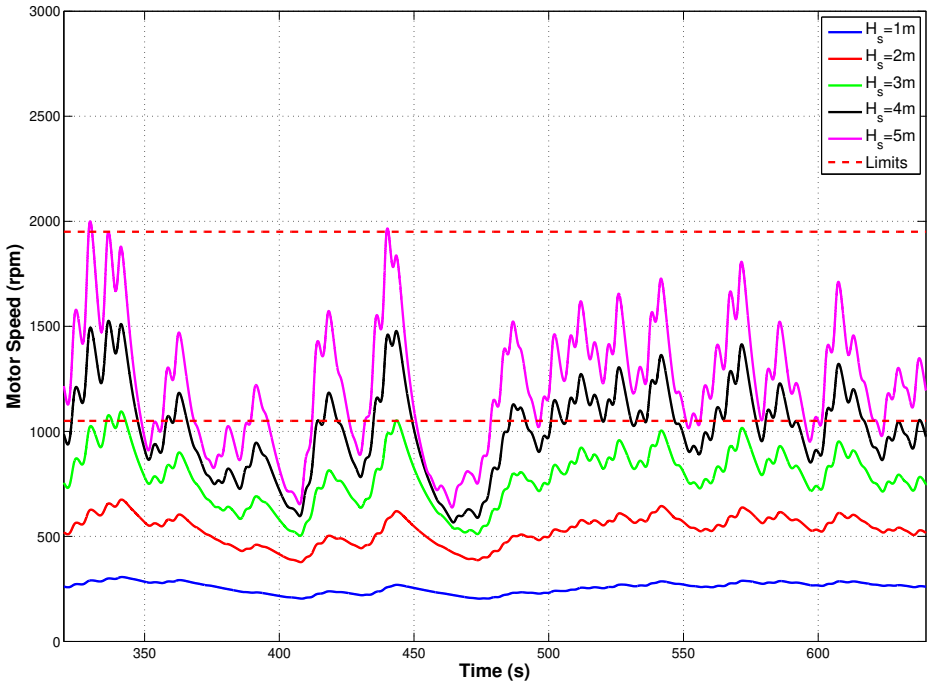

Figure 10: Hydraulic Motor speed vs time for different significant wave heights for an optimally tuned PTO. ($T_p = 11\,\mathrm{s}$)

H_s (m)	Power (kW)		$\eta_{trans}(\%)$	Speed (rpm)	
	P_{gen}	P_{trans}		$\bar{\omega_m}$	ω_{var}
1	1.25	0	0	256.3	103.2
2	5.43	0	0	530.4	298.0
3	12.03	0.37	3.1	783.3	592.3
4	20.43	11.97	58.6	1012.5	960.1
5	30.42	25.59	84.1	1227.6	1362.5

Table 4: Table showing effects of significant wave height on generated power, transmitted power, average motor speed and speed variation. ($T_p = 11\,\mathrm{s}$)

Figure 10 displays the motor speed for an optimally tuned PTO in five different significant wave heights of the same wave spectrum. H_s is varied by multiplying the wave amplitude by the appropriate scalar. Figure 10 and Table 4 illustrate

that the magnitude of the motor speed increases with H_s. They also reveal that although the accumulators are large, this does not provide sufficient power smoothing to produce a constant motor speed and the speed variation (ω_{var}) is amplified in larger waves. This means that the motor speed is not always within the operational limits (1050 - 1950 rpm) of the DFIG so, at each H_s, only a certain percentage of P_{gen} can be transmitted to the grid.

For H_s <3 m the motor speed does not reach the lower speed limit so all of P_{gen} is wasted. For $H_s = 3$ m the motor speed only reaches the lower speed limit for a few seconds of the wave cycle so P_{trans} is negligible. However, for H_s >3 m the motor speed is within the limits for a significant portion of the wave cycle so P_{trans} reaches meaningful levels. Results show that the highest η_{trans} of 84% is for $H_s = 5$ m but even for this wave height the average motor speed ($\bar{\omega_m}$) is still less than 1500 rpm.

It would obviously be desirable for $\eta_{trans} = 100\%$, so no power generated by the PTO is wasted. To do this it is necessary to maintain the hydraulic motor speed within the generator speed limits at all times in all wave conditions. To control the motor speed the fraction of motor displacement (x_m) must be adjusted. A proportional-integral controller, with proportional and integral gains of 0.05 and 0.01 respectively, is used to adjust x_m according to the error in speed from the synchronous value with 0.1< x_m <1.0. This change in x_m will not be instantaneous as the swash plate positioning system of the hydraulic piston motor will have its own dynamics. It is assumed that these dynamics can be modelled as a first order transfer function ($R(s)$) with a time constant, $\tau = 0.1$ s, such that

$$R(s) = \frac{1}{1 + 0.1s} \tag{44}$$

To ensure P_{cap} remains at its maximum, $\alpha_{opt}(T_p)$ must be maintained whilst controlling the motor speed. To maintain α_{opt} it is necessary to continually adjust the piston area or generator load at the same rate as x_m. Adjusting the generator load is the only feasible option so it must be varied alongside x_m to maintain α_{opt}.

$$C_g = \alpha_{opt}(T_p)\left(\frac{x_m D_m}{A_p}\right)^2 \tag{45}$$

Therefore, in the controller the signal to alter the generator load is passed through the same transfer function ($R(s)$) to ensure both signals are in phase. The block diagram of this control strategy is shown in Figure 11.

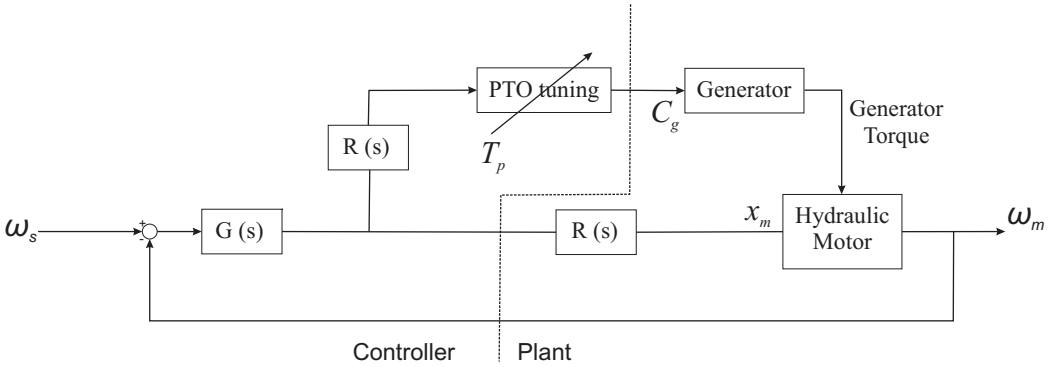

Figure 11: Control Strategy Block Diagram

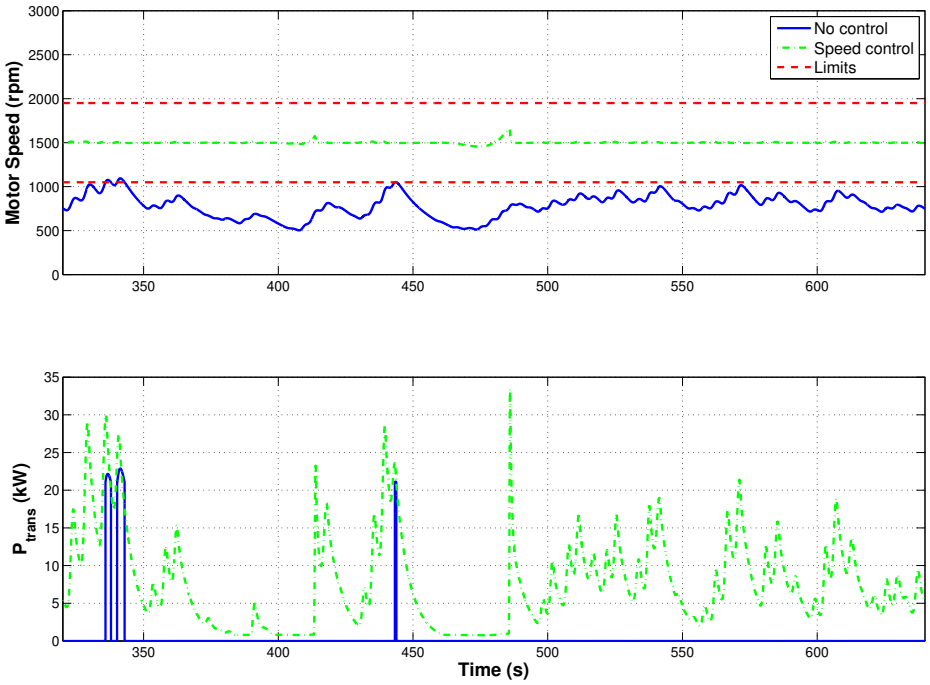

Figure 12: Motor speed and transmitted power with and without speed control. (H_s=3 m and T_p=11 s)

Figure 12 reveals the advantages of implementing a speed control strategy because the hydraulic motor speed remains approximately constant at the

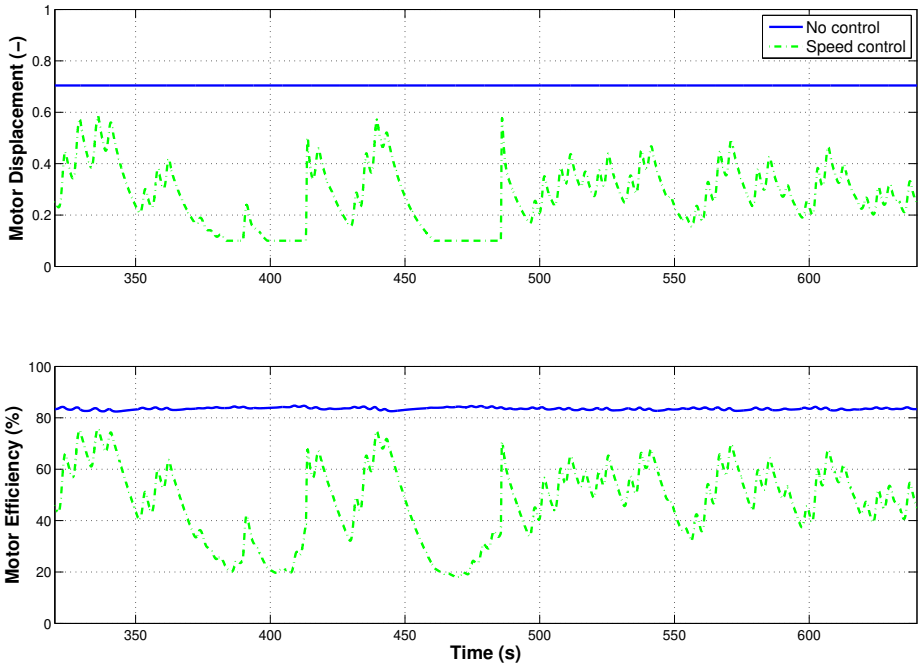

Figure 13: Fraction of motor displacement and motor efficiency with speed control. (H_s=3 m and T_p=11 s)

synchronous speed for the full wave cycle, so $\eta_{trans} = 100\%$. Without speed control the motor speed is highly variable and is rarely within the operational limits, so $\eta_{trans} = 3.1\%$. Because α is constant for both cases, P_{cap} is similar but P_{gen} is 40% lower with the speed control strategy due to the large reduction in motor efficiency (η_m), shown in Figure 13. To maintain the required motor speed, x_m is constantly varying but on average ($\bar{x_m}$) it is at a relatively low value for this wave profile. $\bar{x_m} = 0.47$ and x_m even reduces to the minimum value for parts of the wave profile. η_m exhibits a strong correlation with x_m, and so there is a significant reduction in η_m, and therefore in η_{pto}.

9. Control Strategy Evaluation

The result for the single wave profile shows a large improvement in P_{trans} by implementing a motor control strategy. However, to fully evaluate the improvements, it is necessary to consider a number of sea states (SS). The four sea states shown in Figure 14, created from the parameters in Table 5 are used because they represent a range of wave conditions which the WEC could

encounter. P_{wave} is the total power available in the waves, and for each sea state α_{opt} is obtained from the trend line in Figure 7.

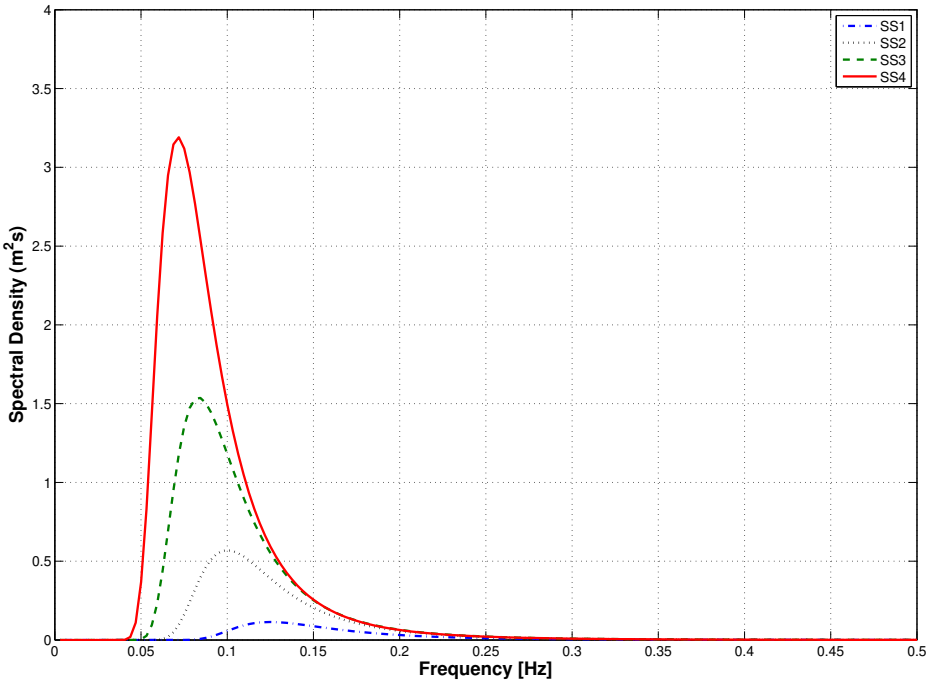

Figure 14: Wave Spectra for the four sea states being investigated

Sea State (SS)	H_s (m)	T_p (s)	P_{wave} (kW)	α_{opt} (kNs/m)
1	1.0	8.0	13.5	145
2	2.0	10.0	67.3	200
3	3.0	12.0	181.7	255
4	4.0	14.0	376.9	310

Table 5: Parameters of the four sea states

For these four sea states, three strategies will be compared:

1. **No PTO tuning and no speed control**- Constant, maximum motor capacity (x_m=1) and constant generator load (C_g). ($\alpha = 100\,\text{kNs/m}$)

2. **PTO tuning and no speed control**- Motor displacement adjusted to give optimum PTO damping for each SS with generator load at maximum value. Both values constant for the simulation. ($\alpha = \alpha_{opt}$)

3. **PTO tuning and closed loop speed control**- Motor displacement and

generator load continually adjusted to maintain optimum PTO damping and provide speed control. ($\alpha = \alpha_{opt}$)

In order to size the hydraulic motor appropriately, information on the wave power at the specific site at which the device will be deployed is required. Here the motor capacity has been reduced by a factor of 3 to 60 cc/rev to ensure $\bar{x_m} \approx 0.8$ for the average wave power. The proportional and integral gains of the controller have been adjusted to 0.45 and 0.09, respectively, to ensure they have the same effect on this smaller motor. In order to maintain $\alpha_{min} = 100\,\text{kNs/m}$, the generator resistance has been reduced so its maximum value is $C_g = 0.19\,\text{Nm/(rad/s)}$.

SS	Power (kW)			Efficiency (%)		
	P_{cap}	P_{gen}	P_{trans}	η_{pto}	η_{trans}	η_{tot}
1	1.70	0.81	0	47.8	0	0
2	7.14	3.52	3.12	49.4	88.4	43.6
3	14.35	6.79	4.28	47.3	63.1	29.8
4	21.52	9.68	3.04	45.0	31.3	14.1

Table 6: Modified PTO Design- Control Strategy 1

SS	Power (kW)			Efficiency (%)		
	P_{cap}	P_{gen}	P_{trans}	η_{pto}	η_{trans}	η_{tot}
1	1.63	0.85	0	51.8	0	0
2	7.45	4.14	3.44	55.6	83.0	46.1
3	14.62	7.97	3.21	54.5	40.3	21.9
4	23.14	11.74	2.27	50.7	19.3	9.8

Table 7: Modified PTO Design- Control Strategy 2

SS	Power (kW)			Efficiency (%)		
	P_{cap}	P_{gen}	P_{trans}	η_{pto}	η_{trans}	η_{tot}
1	0.63	0.02	0.01	3.5	55.1	1.9
2	7.30	4.15	4.15	56.9	100	56.9
3	15.15	9.80	9.80	64.7	100	64.6
4	23.34	15.76	10.94	67.5	69.4	46.9

Table 8: Modified PTO Design- Control Strategy 3

The results for the four sea states comparing the 3 strategies with the modified PTO design are presented in Tables 6, 7 and 8. The power associated with SS1 is negligible so the results for this sea state will not be discussed again.

SS	Strategy 1		Strategy 2		Strategy 3	
	$\bar{x_m}$	$\eta_m(\%)$	$\bar{x_m}$	$\eta_m(\%)$	$\bar{x_m}$	$\eta_m(\%)$
1	1.0	66.3	0.85	69.6	0.1	4.3
2	1.0	61.0	0.72	64.7	0.56	65.2
3	1.0	57.9	0.64	62.1	0.84	74.3
4	1.0	54.8	0.58	59.3	0.89	76.9

Table 9: Motor characteristics for the 3 control strategies with the modified PTO design

With the modified PTO, control strategy 3 performs the best. It gives a similar P_{cap} to strategy 2 but it gives a larger P_{gen}, especially for SS3 and SS4, due to a higher η_m from the increased x_m. Furthermore, due to the speed control, η_{trans} is higher for each SS. These combined effects result in a much larger P_{trans} for each SS using control strategy 3. The advantages are clear to see for SS3 in Figures 15 and 16. It gives the largest overall P_{trans} for the majority of the cycle because the motor speed is always within the limits and the motor efficiency is generally higher so the magnitude of P_{trans} is also predominantly higher.

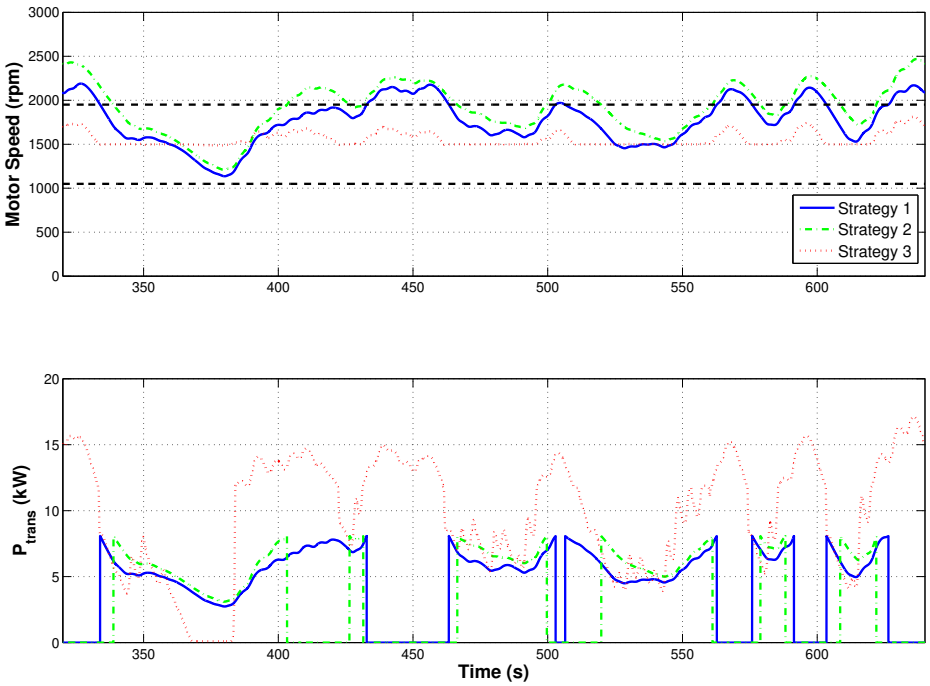

Figure 15: Motor speed and transmitted power for the 3 control strategies in SS3 with the modified PTO design

Table 10 provides a summary of the results for this strategy for both PTO designs and it reveals the benefits of the smaller hydraulic motor and generator

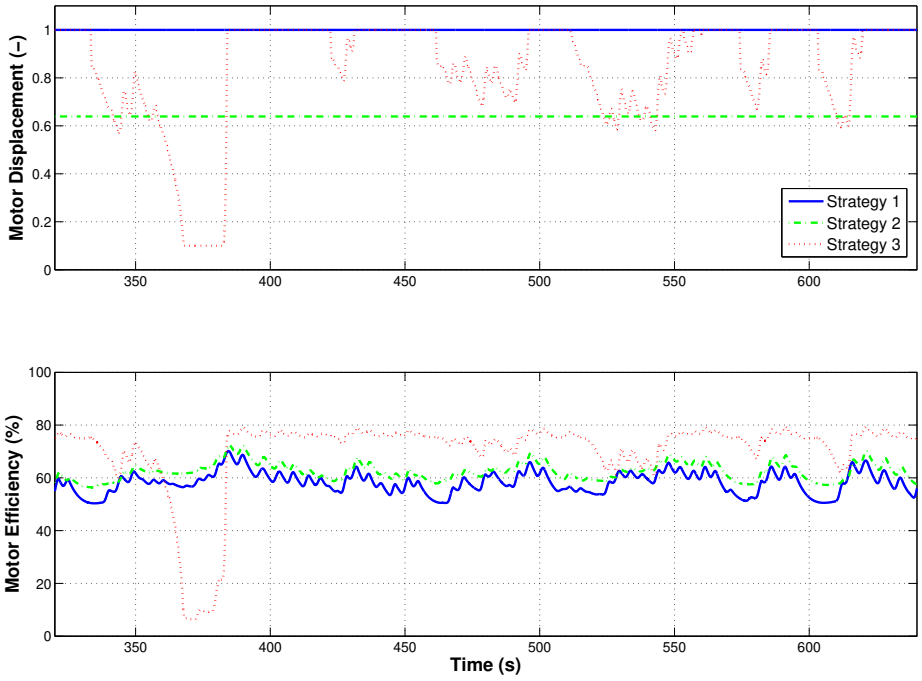

Figure 16: Fraction of motor displacement and motor efficiency for the 3 control strategies in SS3 with the modified PTO design

load in the modified PTO. There is an increase in P_{cap} for each SS compared to the initial PTO, especially for SS2. This indicates a better tuned PTO and an increase in power capture efficiency. P_{gen} is also higher for each SS due to the higher η_m from the increased $\bar{x_m}$. Figure 17 displays these improvements. It shows that for the both PTOs, the motor speed does not remain constant in SS3 because the motor capacity is either too large for the initial PTO or too small for the modified PTO, to maintain the synchronous speed for certain flows. However, the motor speed remains within the operational limits for both PTOs during these periods so importantly no power is lost. However, P_{trans} is higher for the modified PTO mainly because of the increased η_m, shown in Figure 18. All these combined improvements mean a significant increase in P_{trans} for SS2 (43%) and SS3 (50%). For SS4 there is a small reduction (15%) in P_{trans} due to the reduced η_{trans} but this loss is limited by the increase in η_{pto}. In larger waves the smaller capacity motor can not continually maintain the motor speed within the required range so the upper limit is exceeded for a short period of time. Overall though, it is predicted that SS4 will be less frequent than SS2 and SS3,

so when all sea conditions are considered, the modified PTO will provide significant gains in transmitted power.

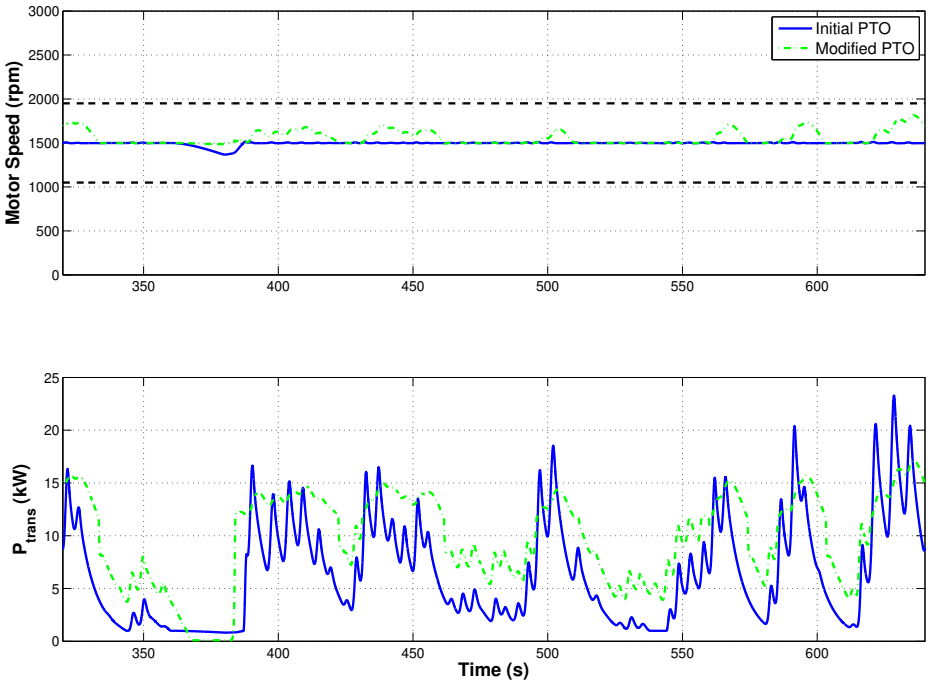

Figure 17: Motor speed and transmitted power for initial and modified PTO design in SS3

SS	P_{wave}	Initial PTO			Modified PTO		
		P_{cap}	P_{trans}	$\eta_{tot}(\%)$	P_{cap}	P_{trans}	$\eta_{tot}(\%)$
2	67.3	5.26	0.78	14.8	7.30	4.15	56.9
3	181.7	14.40	6.50	45.2	15.15	9.80	64.6
4	376.9	23.07	12.89	55.9	23.34	10.94	46.9

Table 10: PTO comparison with control strategy 3

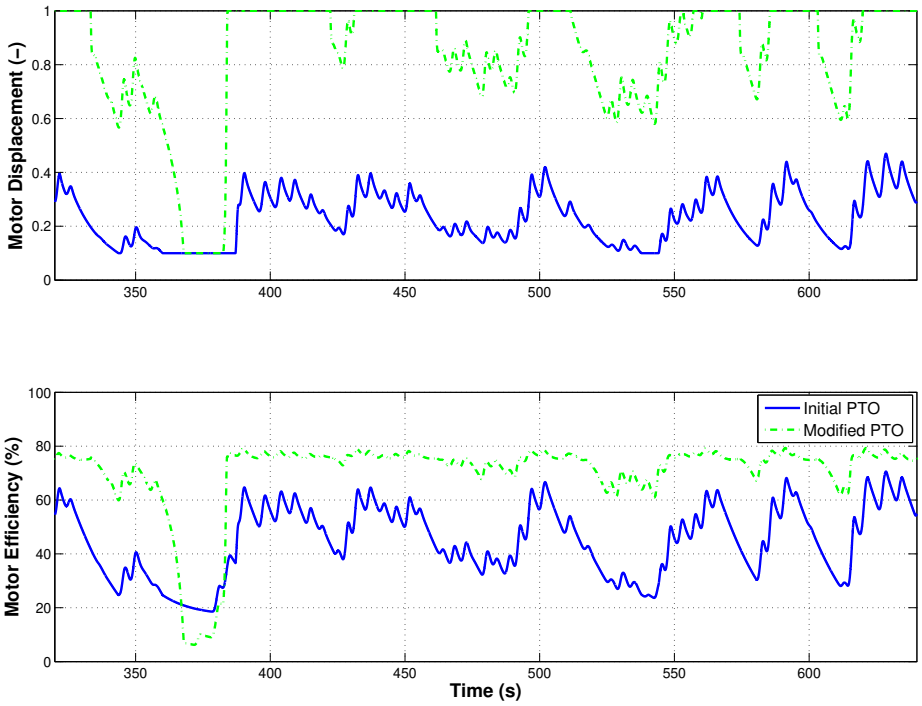

Figure 18: Fraction of motor displacement and motor efficiency for initial and modified PTO design in SS3

10. Conclusions

Using the Pierson-Moskowitz spectrum, the random phase method was applied to create the wave elevation and excitation force profile to represent an irregular wave. Using this input the behaviour of a point absorber WEC with a hydraulic PTO was examined. As expected, no pseudo steady state is reached and the behaviour of the device is very changeable. Induced body stall occurs but the period of stall is varying. The pressure and volume of the accumulators to continuously vary in an attempt to maintain a relatively constant motor speed. In terms of tuning, a linear trend between optimum PTO damping and peak wave period is observed but values differ from those for a regular wave input [2]. The power captured by the hydraulic PTO is low in comparison to regular waves of the same wave height.

Consideration was given to how the mechanical power generated by the PTO would be transmitted into electrical energy. It was assumed that a doubly fed induction generator (DFIG) would be used, as in wind turbines. It was assumed that power is transmitted if the speed of the hydraulic motor is within the range of $\pm$ 30% of the generator synchronous speed. A feedback controller is therefore needed to maintain the motor speed within these limits by altering the fraction of motor displacement. The generator load must also be altered to maintain optimum PTO damping and ensure maximum power capture.

The gains in transmitted power resulting from the use of motor speed control are clear but, due to the low flows and large hydraulic motor in the original design, the fraction of motor displacement is very low for all of the sea states investigated. This causes a low motor efficiency, a low PTO efficiency and a reduction in power capture, which all amounts to a reduction in generated power. Therefore, in an attempt to increase PTO efficiency, a smaller hydraulic motor and generator load was introduced. This was found to increase the transmitted power for most sea states by increasing the capture, PTO and transmission efficiency. There was a slight decrease in the transmitted power for the largest sea state but this sea state is expected to be less frequent so overall there will be significant power gains for the device.

These results show that the motor efficiency has a big effect on the transmitted power. If motor control is implemented, the full range of motor displacement is utilised in all sea states to maintain the generator synchronous speed. Hydraulic motor efficiency exhibits a strong correlation to part displacement so it would be desirable to maintain a constant, high motor efficiency for all displacements. Therefore, ideas such as generating modules with smaller motors that can be switched in and out depending on the incoming wave power have been proposed [21] but no results have been published. Likewise, Digital Displacement ® pumps and motors have been developed to increase efficiency, especially at part load, so they are a possible solution to this problem because they would allow a larger motor to be implemented whilst not compromising the motor efficiency at part load [22]. Moreover, a combination of the two could give the best overall solution. Finally, it is worth noting that even with this control strategy, optimal PTO tuning and a more efficient PTO design, the power levels are still relatively low for a device of this size and the generator losses have not been included.

References

[1] A.R. Plummer and M. Schlotter. Investigating the Performance of a Hydraulic Power Take-Off. In *Proceedings of the 8th European Wave and Tidal Energy Conference (EWTEC)*, Uppsala, Sweden, 2009.

[2] CJ Cargo, AR Plummer, AJ Hillis, and M Schlotter. Determination of optimal parameters for a hydraulic power take-off unit of a wave energy converter in regular waves. *Proceedings of the Institution of Mechanical Engineers, Part A: Journal of Power and Energy*, 226(1):98–111, 2012.

[3] A.F.O. Falcão. Modelling and control of oscillating-body wave energy converters with hydraulic power take-off and gas accumulator. *Ocean Engineering*, 24:2021–2032, 2007.

[4] A.F.O. Falcão. Phase control through load control of oscillating-body wave energy converters with hydraulic PTO system. *Ocean Engineering*, 35:358–366, 2008.

[5] A. Babarit, G. Duclos, and A.H. Clément. Comparison of latching control strategies for a heaving wave energy device in random sea. *Applied Ocean Research*, 26(5):227–238, 2005.

[6] H. Yavuz, A. McCabe, G. Aggidis, and M.B. Widden. Calculation of the performance of resonant wave energy converters in real seas. *Proceedings of the Institution of Mechanical Engineers, Part M: Journal of Engineering for the Maritime Environment*, 220(3):117–128, 2006.

[7] H. Yavuz, T.J. Stallard, A.P. McCabe, and G. Aggidis. Time series analysis-based adaptive tuning techniques for a heaving wave energy converter in irregular seas. *Proceedings of the Institution of Mechanical Engineers, Part A: Journal of Power and Energy*, 221(1):77–90, 2007.

[8] M. Folley and T. Whittaker. The control of wave energy converters using active bipolar damping. *Proceedings of the Institution of Mechanical Engineers, Part M: Journal of Engineering for the Maritime Environment*, 223(4):479–487, 2009.

[9] A. Babarit, M. Guglielmi, and A.H. Clément. Declutching control of a wave energy converter. *Ocean Engineering*, 36:1015–1024, 2009.

[10] J. Falnes. *Ocean Waves and Oscillating Systems*. Cambridge University Press, Cambridge, UK, 2002.

[11] A. Hulme. The Wave forces acting on a floating hemisphere undergoing forced periodic oscillations. *The Journal of Fluid Mechanics*, 121:443–463, 1982.

[12] S. Barstow, D. Mollison, and J. Cruz. The Wave Energy Resource. In J. Cruz, editor, *Ocean Wave Energy: Current Status and Future Perspectives*, chapter 4, pages 93–132. Springer, 2008.

[13] R. Henderson. Design, simulation, and testing of a novel hydraulic power take-off system for the Pelamis wave energy converter. *Renewable Energy*, 31(2):271–283, February 2006.

[14] W.E. Wilson. Performance criteria for positive displacement pumps and fluid motors. *Trans. Am. Soc. Mech. Eng*, 71(2), 1949.

[15] Y. Goda. Statistical Properties and Spectra of Sea Waves. In *Advanced Series And Design Of Maritime Structures*, volume 15, chapter 2, pages 12–44. 2000.

[16] W.J. Jr Pierson and L. Moskowitz. A proposed spectral form for fully developed wind seas based on the similarity theory of S.A. Kitaigoroskii. *Journal of Geophysical Research*, 69(24):5181–5190, 1964.

[17] M.J. Ketabdari and A. Ranginkaman. Simulation of Random Irregular Sea Waves for Numerical and Physical Models Using Digital Filters. *Transaction B: Mechanical Enginerring*, 16(3):240–247, 2009.

[18] AJ Hillis. Active motion control of fixed offshore platforms using an extended state observer. *Proceedings of the Institution of Mechanical Engineers, Part I: Journal of Systems and Control Engineering*, 224(1):53–63, 2010.

[19] A.P. McCabe and G.A. Aggidis. Optimum mean power output of a point-absorber wave energy converter in irregular waves. *Proceedings of the Institution of Mechanical Engineers, Part A: Journal of Power and Energy*, 223(7):773–781, 2009.

[20] A. Petersson. *Analysis, Modeling and Control of Doubly-Fed Induction Generators for Wind Turbines*. PhD thesis, Chalmers University of Technology, 2005.

[21] K. Schlemmer, F. Fuchshumer, N. Böhmer, R. Costello, and C. Villegas. Design and Control of a Hydraulic Power Take-off for an Axi-symmetric Heaving Point Absorber. In *Proceedings of the 9th European Wave and Tidal Energy Conference (EWTEC)*, Southampton, UK, September 2011.

[22] R. Costello, J.V. Ringwood, and J. Weber. Comparison of Two Alternative Hydraulic PTO Concepts for Wave Energy Conversion. In *Proceedings of the*

9th European Wave and Tidal Energy Conference (EWTEC), Southampton, UK, September 2011.

Nomenclature

$A(\omega)$	frequency dependent added mass	[kg]
A_p	piston area	[m^2]
a	buoy radius	[m]
B_o	bulk modulus of hydraulic fluid	[bar]
$B(\omega)$	frequency dependent radiation damping coefficient	[Ns/m]
C_f	motor coulomb friction coefficient	[-]
C_g	generator damping coefficient	[Nm/(rad/s)]
C_s	motor slip coefficient	[-]
C_v	motor viscous friction coefficient	[-]
D_m	motor capacity	[cc/rev]
E_A	accumulator 'A' energy	[J]
E_B	accumulator 'B' energy	[J]
E_m	motor energy	[J]
f_c	coulomb friction	[N]
f_e	wave excitation force	[N]
f_{fr}	cylinder friction	[N]
f_h	wave force	[N]
f_{hs}	wave hydrostatic force	[N]
f_v	viscous friction coefficient	[Ns/m]
f_r	wave radiation force	[N]
$F_e(s)$	Laplace transform of wave excitation force	[N]
g	gravitational acceleration	[ms^{-2}]
H	wave height	[m]
H_s	significant wave height	[m]
J	generator inertia	[kgm^2]
K_v	valve coefficient	[$m^3/s\,bar$]
k	wave number	[m^{-1}]
l	half height of buoy	[m]
m	mass of buoy	[kg]
n	number of wave components	[-]
p_i	piston chamber pressure (i = 1,2)	[bar]
p_A	accumulator 'A' pressure	[bar]
p_B	accumulator 'B' pressure	[bar]
p_o	initial accumulator pressure	[bar]
$\bar{P}_{cap}$	average captured power	[kW]
P_{cap}	captured power	[kW]
P_{gen}	generated power	[kW]

P_{trans}	transmitted power	[kW]
P_{wave}	wave power	[kW]
q	flow rate	[m^3/s]
q_m	flow rate to the motor	[m^3/s]
S	buoy cross sectional area	[m^2]
S_n	spectral density	[m^2s]
t	time	[s]
T_m	motor torque	[Nm]
T_p	peak period	[s]
V_i	piston chamber oil volume (i = 1,2)	[m^3]
V_A	accumulator 'A' oil volume	[m^3]
V_B	accumulator 'B' oil volume	[m^3]
V_o	initial oil volume in accumulators	[m^3]
x	buoy displacement	[m]
x_m	fraction of motor displacement	[-]
$\bar{x_m}$	average fraction of motor displacement	[-]
α	PTO damping	[Ns/m]
α_{opt}	optimum PTO damping	[Ns/m]
Δt	wave cycle time	[s]
$\Delta\omega$	wave frequency band	[rad/s]
ϵ	Havelock's coefficient	[-]
η	wave surface elevation	[m]
η_m	motor efficiency	[%]
η_{pto}	PTO efficiency	[%]
η_{tot}	total PTO efficiency	[%]
η_{trans}	transmission efficiency	[%]
γ	adiabatic index	[-]
$\Gamma(\omega)$	wave excitation force coefficient	[N/m]
μ	oil dynamic viscosity	[Ns/m^2]
ρ	water density	[kg/m^3]
ρ_o	oil density	[kg/m^3]
Φ	PTO force	[N]
ω	wave frequency	[rad/s]
ω_m	angular motor velocity	[rad/s]
$\bar{\omega_m}$	average motor angular velocity	[rad/s]
ω_{max}	maximum frequency	[rad/s]
ω_{min}	minimum frequency	[rad/s]
ω_{var}	motor speed variation	[rad/s]
φ	wave phase component	[s]